

Puzzling out the ecological niche construction for nitrogen fixers in a coastal upwelling system

3 Marcos Fontela¹, Daniel Fernández Román², Esperanza Broullón³, Hanna Farnelid⁴, Ana
4 Fernandez Carrera⁵, Emilio Marañón², Sandra Martínez García², Tamara Rodríguez-
5 Ramos⁶, Marta Varela⁶, Beatriz Mouríño²

6 Corresponding autor: mfontela@iim.csic.es

7

8 ¹Instituto de Investigación Mariñas (IIM-CSIC), Vigo, Spain

⁹ ²Centro de Investigación Mariña da Universidade de Vigo (CIM-UVIGO), Vigo, Spain

¹⁰Ocean and Earth Science, National Oceanography Centre, University of Southampton,
¹¹Southampton, UK

12 ⁴Department of Biology and Environmental Science, Centre for Ecology and Evolution in
13 Microbial Model Systems (EEMiS), Linnaeus University, Kalmar, Sweden

⁵ Instituto de Oceanografía y Cambio Global, Universidad de Las Palmas de Gran Canaria (ULPGC), 35214, Las Palmas, Spain.

¹⁶Centro Nacional Instituto Español de Oceanografía, (IEO-CSIC), Centro Oceanográfico
¹⁷de A Coruña, Paseo Marítimo Alcalde Francisco Vázquez, nº 10, 15001, A Coruña, Spain.

Competing Interests statement: The authors declare no competing financial interests.

Keywords: biological nitrogen fix

20 upwelling, nitrogen limitation

21

22 **Abstract**

23 Diazotrophs are a diverse group of microorganisms that can fertilize the ocean through
24 biological nitrogen fixation (BNF). Due to the high energetic cost of this process, diazotrophy
25 in nitrogen-replete regions remains enigmatic. We use multidisciplinary observations to
26 propose a novel framework for the ecological niche construction of nitrogen fixers in the
27 region off NW Iberia— one of the most productive regions in Europe, characterized by weak,
28 and intermittent wind-driven upwelling and the presence of bays. The main diazotroph
29 detected (UCYN-A2) was more abundant and active during summer and early autumn,
30 coinciding with relatively high temperatures ($>16^{\circ}\text{C}$), low nitrogen:phosphorus ratios (N:P
31 <0.45), and a large contribution of ammonium ($>75\%$) to the total inorganic nitrogen
32 available. Furthermore, nutrient amendment experiments showed that BNF is detectable
33 when phytoplankton assemblages are nitrogen limited. Seasonally recurrent
34 biogeochemical processes driven by hydrography create the ecological niche for nitrogen
35 fixers in this system. During the spring-summer upwelling, non-diazotrophs autotrophs
36 produce organic matter inside the bays and promote nitrate drawdown. Thereafter, the
37 combined effect of intense remineralization on the shelf and sustained positive circulation
38 within the bays in late summer-early autumn, conveys enhanced ammonium content and
39 excess phosphate into the warm surface layer. The low N:P ratio confers a competitive
40 advantage to diazotrophs since they are not restricted by nitrogen supply. These results
41 could help to explain why the upwelling bays are more productive compared to the upwelled
42 offshore waters, as this process could be at play in other temperate upwelling regions
43 traditionally overlooked for BNF.

44

45

Introduction

46 Nitrogen (N) is a key element in the biosphere which limits the growth of primary producers
47 in marine and land ecosystems[1]. Despite being very abundant in the atmosphere, it is only
48 available for a reduced group of organisms, termed diazotrophs, able to reduce atmospheric
49 dinitrogen (N_2) gas into biologically assimilable forms, through biological nitrogen fixation
50 (BNF). The traditional focus on archetypal marine N_2 -fixers (filamentous cyanobacteria and
51 diatom-diazotroph associations) has been expanded to include unicellular cyanobacteria
52 and multiple groups of heterotrophic bacteria and Archaea[2]. While the BNF activity of some
53 of these groups is still uncertain or reduced[3], the small diazotrophic cyanobacteria
54 *Candidatus Atelocyanobacterium thalassa* (hereafter UCYN-A) has emerged as a key player
55 in the marine nitrogen cycle[4], showing characteristics of a N_2 -fixing organelle, or
56 “*nitroplast*”[5].

57 Despite decades of intense research, the control factors of diazotrophy remain enigmatic. It
58 was traditionally assumed that the ability to access the vast atmospheric N_2 pool gives
59 ecological advantage to diazotrophs where and when fixed N concentrations are low,
60 whereas BNF would be irrelevant at enhanced availability of combined N resources[2].
61 However, energetically, fixing N_2 is only marginally (~25%) more costly than using nitrate[6],
62 and recent studies have expanded diazotroph global distribution to N-enriched regions[7–10],
63 including subpolar and polar waters[11–14], coastal zones [15–17], upwelling ecosystems
64 [18–20], and even the aphotic ocean[21].

65 Methodological approaches to investigate the relevance of control factors on diazotrophy
66 include modeling studies[22, 23], nutrient addition experiments in the lab or with natural
67 populations [6, 24, 25], and database analyses to explore relationships between
68 environmental variables and the presence or activity of diazotrophs[10]. However,
69 deciphering the independent effect of environmental properties on the distribution and

70 activity of diazotrophs is not trivial. First, because environmental conditions are correlated
71 to each other, and second because nutrient concentration does not necessarily inform about
72 nutrient availability, since low concentrations can be the result of phytoplankton
73 consumption[26]. Few studies have investigated the drivers of diazotrophy in N-enriched
74 regions, revealing correlations with temperature, chlorophyll-a (*Chla*) and inorganic nutrient
75 content[9, 18, 27]. Whether these relationships are circumstantial or the result of control
76 mechanisms for diazotrophy, remains enigmatic.

77 The coastal upwelling region off the western Iberian Peninsula marks the northern limit of
78 the Canary Current Upwelling Ecosystem, characterized by coastal embayments known as
79 Rías[28]. In this area, upwelling is weak and intermittent, and the Rías are considered an
80 extension of the shelf[29]. The predominance of along-shore northeasterly winds in
81 spring/summer causes seasonal upwelling and positive circulation— surface waters from
82 the Rías moves towards the ocean, while deeper, nutrient-rich oceanic waters flow into the
83 Rías [30, 31]. These nutrient inputs, enhanced by remineralization within the Rías and on
84 the shelf[32], drive, among other factors, high phytoplankton production, which supports one
85 of the most important blue economies in Europe [33]. During early spring, when nutrient
86 availability is high, the phytoplanktonic community is dominated by large diatoms and
87 autotrophic nanoflagellates[34], while smaller diatoms and heterotrophs coexist during
88 summer, as regenerated nutrients become more significant [35]. From October to March,
89 prevailing southerly winds promote downwelling events[30, 31] and negative circulation —
90 where surface waters flow into the Rías while deeper waters are expelled - associated with
91 low phytoplankton growth conditions[36].

92 Knowledge about diazotrophy in this region is limited to a few observations. Relatively low
93 BNF rates, mainly attributed to UCYN-A, were reported in the shelf off Ría de Vigo in
94 summer of 2009[37, 38]. Ten samplings carried out between February 2014 - December

95 2015 at the shelf off Ría de A Coruña confirmed relatively low BNF rates in the region, which
96 were higher (up to $0.095 \text{ nmol N L}^{-1}\text{d}^{-1}$) in surface waters during summer upwelling and
97 relaxation[20]. Under these conditions the diazotroph community was dominated by UCYN-
98 A2, whereas with downwelling non-cyanobacterial diazotrophs (i.e. heterotrophic Bacteria
99 and Archaea, hereafter NCD) were dominant[19]. Despite these insights, the factors driving
100 BNF in this system remain unknown, as the limited temporal resolution of previous studies
101 does not allow to reconstruct the environmental conditions accompanying the variability in
102 diazotrophic composition and activity. Here, using a large data set of multidisciplinary
103 observations, we describe in detail the ecological niche construction of nitrogen fixers in the
104 upwelling region off NW Iberia.

105 Materials and methods

106 Sampling and hydrography

107 The dataset comprises 79 one-day sampling events within a period of ~4.5 years (2014-
108 2018). All samples belong to four different locations (Fig. S1). There were 10 samplings from
109 the northern limit of the upwelling system, taken in the adjacent shelf off Ría de A Coruña
110 ($43.42^\circ \text{ N}, 8.44^\circ \text{ W}, 80 \text{ m depth}$) between February 2014 and December 2015
111 (NICANOR[20]). Next, there were 55 samplings with almost weekly resolution at a central
112 station in the inner Ría de Vigo ($42.24^\circ \text{ N } 8.78^\circ \text{ W}, 40 \text{ m depth}$) between March 2017 and
113 April 2018 (REMEDIOS-seasonal[39]). Finally, there were 14 samplings along two weeks of
114 summer 2018 with daily resolution (REMEDIOS-cruise[40]). Among them, 10 samples were
115 taken inside the Ría de Pontevedra ($42.36^\circ \text{N } 8.78^\circ \text{W}, 30 \text{ m depth}$) and 4 from the outer shelf
116 ($42.30^\circ \text{N } 9^\circ \text{W}, \sim 19.6 \text{ km apart}, 100 \text{ m depth}$). During each sampling profiles of temperature,
117 salinity and fluorescence were acquired with a SBE25plus CTD (SeaBird Electronics).
118 Surface samples (1-3 m) were collected to determine dissolved inorganic nutrients

119 (ammonium NH₄, nitrite NO₂, nitrate NO₃⁻, phosphate PO₄), chlorophyll a (*Chla*), primary
120 production (PP), BNF and DNA and RNA samples.

121 Samples for the determination of dissolved inorganic nutrients and total *Chla* were collected
122 and frozen at -20°C [41, 42]. The fluorescence emitted by the *Chla* was measured from
123 pigments extracted in 90% acetone at 4°C overnight using the spectrofluorometric
124 method[20], and a Turner designs Trilogy fluorometer [43]. Seawater samples were spiked
125 with 2–10 µCi of NaH¹⁴CO₃ and incubated during 2-3 h starting at noon (REMEDIOS and
126 nutrient addition experiments) or 24 h (NICANOR) in refrigerated incubators simulating the
127 corresponding *in situ* irradiance. More detailed methodological procedures along with
128 comprehensive hydrographic descriptions for each of the sites and conditions can be found
129 in[20, 39, 40]. Since biological samples were restricted to surface, the environmental
130 parameters included as factors in subsequent statistical analysis are the median value of
131 the first 5 meters of the water column. Inorganic nutrient information has also been
132 interpreted in terms of the Redfield normalized N:P ratio:

133
$$\text{N:P ratio} = (\text{NO}_3^- + \text{NO}_2 + \text{NH}_4) / 16^*\text{PO}_4$$

134 A N:P ratio = 1 denotes the fulfillment of Redfield stoichiometry[44]. Deviations from this
135 ratio provide insights into the nutrient availability: N:P>1 denotes excess nitrogen over
136 phosphorus availability, whereas N:P<1 indicates potential nitrogen limitation and excess
137 phosphate. The fraction of NH₄ in total dissolved inorganic nitrogen DIN [%NH₄=NH₄/ (NO₃⁻
138 + NO₂ + NH₄)], expressed as percentage, was the variable informing about nitrogen
139 speciation.

140 **Biological nitrogen fixation rates**

141 Estimates of BNF activity at surface (1-2 m) are available for 34 sampling dates (43% of
142 total samplings). BNF rates were determined with the ¹⁵N₂ bubble addition technique[45].
143 The bottles were sealed with silicone septa caps and 3 mL of ¹⁵N₂ (98 atom%, Cambridge

144 Isotope Laboratories, Lot #I-16727 and #I-19168) were injected with a gas-tight syringe. The
145 bottles were gently mixed, and incubated for 24 hours simulating *in situ* conditions of
146 temperature and light with running-surface water and neutral-mesh shading to mimic surface
147 irradiance. After incubation, each sample was filtered through pre-combusted (4h, 450°C)
148 25 mm Whatman GF/F filters, (0.7 µm nominal pore size) using low vacuum (<100mmHg),
149 and filters were stored frozen (-20°C). A time-zero bottle was also filtered to calculate the
150 initial natural abundance of N isotopes in the particulate material. Before analysis, filters
151 were thawed, dried (60°C, 24-48 h) and pelletized in tin capsules. Particulate organic
152 nitrogen and carbon (PON and POC) content, as well as the relative abundance of stable
153 nitrogen isotopes ($^{15}\text{N}/^{14}\text{N}$) were determined with a continuous-flow isotope-ratio mass
154 spectrometer MAT253 (Thermo Finnigan) coupled to an elemental analyser EA1108 (Carlo
155 Erba Instruments) through a Conflo III interface (Thermo Finnigan). During analysis, a set
156 of international reference materials were analyzed for $\delta^{15}\text{N}$ calibration (USGS 40,
157 USGS41a USGS-25, IAEA-N-1, and IAEA-N-2). An analytical measurement error of \pm
158 0.15‰ was calculated for $\delta^{15}\text{N}$; the error estimate was obtained from replicate assays of
159 the laboratory standard acetanilide interspersed between sample analysis. Detection limits
160 and error propagation were evaluated[46].

161 **Nutrient addition experiments with natural planktonic communities**
162 Four nutrient addition experiments were performed (coinciding with different climatological
163 seasons of 2017) along with the *in situ* sampling of natural planktonic communities at the
164 inner part of Ría de Vigo (Fig. S1). Experimental design included a control (no additions
165 performed) and two addition treatments: i) NO_3^- treatment, amended with 10-15 µM NO_3^-
166 and ii) NH_4^+ treatment, amended with 10-15 µM NH_4^+ . Besides, 1 µM of phosphate (PO_4^{3-}),
167 and a mix of organic nutrients (5 µM glucose and 5 µM amino acids) were included in both
168 addition treatments. A detailed description of the experimental setup is available in Text S1.

169 Experiments lasted 3 days and samples were taken every 24 h to monitor changes in *Chla*
170 and PP. Samples for RNA and BNF rates were collected after 24 h incubation. The
171 magnitude of the responses was estimated as response ratios (RR) between the time-
172 integrated value of the variable over the incubation time in the amendment treatment (AT)
173 and the control (C), AT/C. In the case of biomasses, time-averaged values were used.

174 Bulk DNA sampling, extraction, nested-amplification of the *nifH* gene
175 and Illumina sequencing

176 For 71 sampling dates (90% of total) surface water was sampled for DNA collection.
177 Between 7.5 and 10 L of seawater per replicate (4 replicates) were collected and filtered
178 using silicone tubes and peristaltic pumps through sterile STERIVEX 0.22 µm pore size
179 filters (Millipore, USA). Summer samples of July 2018 were prefiltered with a 200 µm mesh
180 filter. Filters were preserved with 1.8 mL of lysis buffer (50 mM Tris-HCl pH 8.3, 40 mM
181 EDTA pH 8.0, 0.75 M sucrose), immersed in liquid nitrogen and subsequently stored at -80
182 °C until further analysis. DNA was extracted using the PowerWater® DNA Isolation Kit
183 (Mobio, Carlsbad, CA, USA.), quantified and quality-checked (according to the A260/A280
184 ratio) using a spectrophotometer NanoDrop 2000TM (Thermo Fisher Scientific).
185 Amplification of *nifH* gene and sequencing of the amplicons were performed following [47,
186 48]. The PCR reactions were run on a T100TM Thermal cycler (BIO-RAD)[19]. The amplified
187 products were purified using PCR Extract Mini Kit (5PRIME) and quantified using a
188 spectrophotometer NanoDrop 2000™ (Thermo Fisher Scientific). Prior to sequencing, an
189 additional PCR amplification of 10 cycles with custom barcoded *nifH1* and *nifH2* primers
190 was carried out. After purification and library preparation from the barcoded PCR products,
191 paired-end sequencing was performed using the MiSeq® reagent kit with V2 chemistry (500
192 cycles) at the facilities of IMGM Laboratories GmbH (Germany) on the Illumina MiSeq® Next
193 Generation Sequencing technology (Illumina Inc.).

194 RNA extraction, cDNA generation and *nifH* gene quantification
195 For 14 sampling dates (18% of total) surface water was sampled for RNA collection following
196 the same procedure described for DNA. Total RNA extraction from Sterivex® filters was
197 performed by using 200 µm Low binding Zirconium beads (OPS diagnostics) and QIAGEN
198 RNeasy Mini Kit (Cat.no 74104) and RNase-Free DNase Set (Cat.no 79254). DNase
199 treatment was done with AMBION Turbo DNA free Kit (Invitrogen, Cat.No: AM1907). First-
200 strand cDNA synthesis was done with SuperScript® III First-Strand Synthesis System for
201 RT-PCR, and total RNA concentration was quantified by Nanodrop & Qubit. To quantify *nifH*
202 genes and expression of key diazotrophs identified in the amplicon libraries, 69 and 14
203 samples were amplified and quantified by quantitative polymerase chain reaction (qPCR)
204 and reverse transcription qPCR (RT-qPCR), respectively, using Taqman primer probe sets
205 (PrimeTime qPCR Assays, Integrated DNA Technologies) (see details in[20]). Briefly, the
206 qPCR assays targeted the *nifH* gene of three common diazotrophic strains, namely UCYN-
207 A2[49], UCYN-A1[50], and γ-Proteobacterium affiliated phylotype γ-24774A11[51] (Table
208 S2). The PrimeTime® Gene Expression Master Mix (IDT), DNA/cDNA template, and
209 primers-probe set (0.5 and 0.25 µM final concentrations, respectively) were combined with
210 PCR grade water (Sigma-Aldrich) to create a final reaction volume of 20 µL. Thermal cycling
211 conditions for the qPCR assay consisted of a 3-minute incubation at 95°C, followed by 45
212 cycles of 15 seconds at 95°C and 1 minute at 60°C. Each qPCR run included nine 10-fold
213 serial dilutions of standards that contained the targeted *nifH* fragments (gBlocks® Gene
214 Fragments, IDT), and samples were run in triplicate, while standards were run in duplicate.
215 Reactions were performed in a MyiQ2™ Real-Time PCR Detection System (Bio-Rad
216 Laboratories). Amplification efficiencies were always greater than 90%. We performed
217 inhibition test by several dilutions at certain random samples and we concluded that our
218 samples were not inhibited. The limit of detection (LOD) was 9 *nifH* copies L⁻¹, and the
219 detected but not quantified (DNQ) limit was 87 *nifH* copies L⁻¹ for UCYN-A2 and UCYN-A1

220 and 86 *nifH* copies L⁻¹ for Gammaproteobacteria. Abundances below LOD were assigned 0
221 *nifH* copies L⁻¹, whereas measurements higher than the LOD but less than the DNQ were
222 assigned 1 *nifH* copies L⁻¹.

223 **Bioinformatics and phylogenetic**

224 Paired-end reads were merged, selected and quality filtered, chimera were removed, and
225 Amplicon Sequence Variants (ASVs) were determined with the *dada2* pipeline[52].
226 Sequences with stop codons or with frameshift errors were excluded from the analysis. Non-
227 *nifH* sequences were filtered out against the database compiled in [53] using the HMMER
228 algorithm. The remaining sequences were aligned to a reference alignment, in the
229 “genome879” *nifH* database (<https://wwwzehr.pmc.ucsc.edu/Genome879/>). The
230 phylogenetic affiliation of the translated ASVs into the canonical *nifH* clusters defined by [54]
231 was performed by BLASTx[55] using genome-derived sequences from the updated and
232 curated *nifH* database[56] as references. Finally, ASVs were sorted according to their
233 closest affiliation in the BLASTp database (>96% cutoff)[54]. Following BLASTp matching
234 at Genus level, diazotrophs were categorized in 9 taxonomical groups (Class level) for
235 subsequent analytical purposes (Table S1). Rarefaction curves (rarefy function in vegan
236 package[57]) showing a plateauing trend (Fig. S2) confirmed that DNA extraction,
237 sequencing and bioinformatics were appropriately implemented for most samples, and only
238 4 DNA samples out of 79 were discarded. We established that the diazotrophic community
239 at each individual sample was dominated by Cyanobacteria when UCYN-A relative
240 abundance met two criteria: i) it was the most abundant ASV and ii) it represented
241 individually more than a third (33%) of total relative abundance. Otherwise, we considered
242 the community dominated by non-cyanobacterial diazotrophs (NCD) (Fig. S3).

243 **Statistical analysis**

244 All statistical analyses were done in R (v4.1.2; R Core Team 2021). The community
245 composition of diazotrophs was investigated by Principal Coordinates Analysis (PCoA,

246 vegan package) with an ordination based on Bray-Curtis dissimilarity distances matrix. The
247 environmental parameters were fitted onto the PCoA ordination and represented as vector
248 overlays when their contribution to the observed differences was relevant (*envfit* function in
249 vegan package, p-value <0.001).

250 Then, we assessed the degree of niche overlap among diazotroph taxonomical groups with
251 respect to those relevant environmental drivers identified from the PCoA (sea surface
252 temperature and N:P ratio). Niche overlap analysis is based on nonparametric kernel density
253 estimation[58, 59]. Based on a null model analysis, the difference in niche overlap between
254 groups was considered statistically significant at a p-value<0.01.

255 Finally, we investigated if those environmental drivers determined ASV's relative
256 abundance. The *corncob* method is based on beta-binomial count regression for correlated
257 observations and is suited for modeling microbial abundances based on high throughput
258 sequencing data[60]. For each individual ASV, a regression model of relative abundance
259 versus environmental data tested the differential abundance across the existent N:P ratio,
260 fraction of NH₄ in total DIN and surface water temperature conditions, also controlling the
261 effect of these environmental drivers on the dispersion. A False Discovery Rate of <0.5%
262 was selected as threshold.

263 Results

264 **Diazotrophic community composition and biological nitrogen fixation**
265 A total of 7030 ASVs were identified based on *nifH* sequencing. The 9 categorized
266 taxonomical groups represented 97.6% of the total ASVs, with *Cyanobacteria* and
267 *Proteobacteria* jointly being 81.6% (45% and 36.6%, respectively) (Fig 1A). The relative
268 abundance of cyanobacterial diazotrophs was large in summer/early autumn while NCD
269 were more relevant in winter/spring, when *Cyanobacteria* were almost absent and the
270 diazotrophic community was more diverse (Fig. S4). UCYN-A2 was the main UCYN-A

271 ecotype and the most abundant ASV. *Deltaproteobacteria* was the second taxa in relative
272 abundance, followed by *Gammaproteobacteria*. The temporal variability of relative
273 abundance based on *nifH* sequencing was coherent with the pattern attained by absolute
274 quantification by qPCR (Fig. 1A, C). Frequently, the quantification of UCYN-A2 was two
275 orders of magnitude larger than UCYN-A1. *Gammaproteobacteria* was below detection limit
276 in more than half of the samples, and their mean absolute abundance was low (708 ± 1600
277 *nifH* gene copies L⁻¹).

278 The mean BNF for all samples was 0.92 ± 1.1 nmol N L⁻¹d⁻¹ (n = 34), from 0.025 nmol N L⁻¹
279 d⁻¹ to 3.17 nmol N L⁻¹d⁻¹ (Fig 1B), and it was below detection (i.e, zero) in 11 samples. BNF
280 rates were higher during summer and early autumn in Ría de Vigo and Ría de Pontevedra
281 (2017-2018), whereas there were in general lower in the northernmost location sampled at
282 the shelf off Ría de A Coruña (2014-2015). Higher BNF rates coincided with relatively high
283 *Cyanobacterial* diazotroph gene abundance, whereas NCD dominated the diazotrophic
284 community when BNF rates were undetectable (Fig.1).

285 The abundance of UCYN-A2 *nifH* transcripts (measured by qPCR based on cDNA) exhibited
286 a close, positive linear relationship with BNF rates at rates lower than 1 nmol N L⁻¹d⁻¹ (Fig.
287 2). Above this threshold, a saturation relationship was observed. Transcription of *nifH*
288 associated to UCYN-A2 also scaled linearly along BNF rates, while no relationship was
289 found between BNF rates and UCYN-A1 *nifH* gene copies or transcripts (Fig. 2).

290 Environmental control of diazotroph community structure

291 PCoA analysis confirmed the existence of two groups of samples according to diazotroph
292 community composition (Fig. 3). The first PCoA axis separated samples in which
293 cyanobacterial diazotrophs dominate the community (cyan circles, UCYN-A) from those in
294 which NCD dominated the community (orange squares, NCD). The lower dispersion
295 observed in the UCYN-A group suggests a less diverse phylogenetic community. On the

296 other hand, the larger dispersion of the NCD group[3] suggest higher phylogenetic diversity
297 at the community level. This is confirmed with alpha diversity metrics (Fig. S5). The
298 environmental parameters that most contributed to this community differences are in situ
299 temperature, the fraction of NH₄ in total dissolved inorganic nitrogen (%NH₄), NO₃⁻, N:P ratio
300 and PO₄ (in that order, complete list of environmental variables and the model fitting
301 coefficients available in Table S3). The N:P ratio, NO₃⁻ and PO₄ were negatively associated
302 with temperature and %NH₄ in the ordination space. The dominance of UCYN-A in the
303 community was associated with higher temperature and %NH₄ concurrent with low N:P ratio.

304 Kernel density estimates were used to assess the niche overlap of taxonomical
305 groups in terms of temperature, %NH₄ in DIN, and N:P ratio (Fig. 4A-C, Table S3).
306 *Cyanobacteria* peaked at 16°C, and they were present at the warmest temperature
307 registered (19-20°C), whereas NCD groups like *Bacteroidia* and *Proteobacteria* (*Gamma*-,
308 *Epsilon*- and *Betaproteobacteria*) peaked around 13°C (Fig. 4A). The fraction of ammonium
309 in total dissolved inorganic nitrogen (DIN) was also a differential parameter for cyanobacteria
310 (more present at higher NH₄ proportions, >75%) and NCD (which showed higher abundance
311 at low NH₄ proportions, 25%, Fig. 4B). Finally, *Cyanobacteria* occurred preferentially at low
312 N:P ratio conditions (0.45), when there was potential N limitation and excess P, whereas
313 NCD groups have their peak of occurrence at N:P ratios>1 (Fig. 4C).

314 Additional statistical support at ASV level with beta-binomial count regression
315 models identified 25 ASV differentially-abundant with regard to temperature, 13 ASVs with
316 regard to the fraction of NH₄ in DIN, and 10 ASVs that are differentially-abundant across the
317 N:P ratio (out of the 7030 ASV tested, Fig 4D). Only UCYN-A2 has a significant differential
318 abundance related to the three environmental drivers. UCYN-A2 was the only
319 *Cyanobacteria* ASV with a temperature-mediated response, as well as the only ASV with a

320 positive coefficient for the relevance of NH₄ in the total DIN, and a negative coefficient for
321 the N:P ratio.

322 **Biological nitrogen fixation is driven by inorganic nitrogen availability**
323 We performed controlled nitrogen amendment experiments to assess whether BNF activity
324 occurs when the phytoplankton standing stock is N-limited, across four seasons (winter,
325 spring, summer and autumn) in the inner Ría de Vigo. As reported previously (Fig. 1),
326 amendment experiments showed higher in situ (natural environment) BNF rates (0.025 nmol
327 N L⁻¹d⁻¹ to 3.17 nmol N L⁻¹d⁻¹) in summer and autumn, whereas they were below detection
328 limit in winter and spring (Fig. 5A). A significant (ANOVA, p-value <0.05, Fig. 5A) positive
329 response of PP and Chl a to nitrogen additions (i.e. phytoplankton standing stock was N-
330 limited) was observed in summer and autumn experiments, coinciding with higher BNF in
331 the field (Fig. 5B). In all seasons with measurable BNF activity, BNF rates were inhibited
332 and significantly reduced when ammonium and nitrate were added, respectively (ANOVA,
333 p-value <0.05, Fig. 5A).

334 Discussion

335 UCYN-A2 is the main active N₂-fixer

336 We revealed through alternative approaches that the abundance of diazotrophs shows
337 seasonality in the NW Iberian upwelling system, with UCYN-A2 being most abundant and
338 active during summer and early autumn. High abundances of *nifH* UCYN-A2 transcripts
339 were concomitant with measurable BNF rates, supporting the link between the expression
340 pattern of UCYN-A2 with BNF rates. This agrees with the current knowledge that UCYN-A2
341 is more relevant in coastal waters than UCYN-A1[61, 62], and supports the recognition of
342 UCYN-A2 as the main active diazotroph in temperate upwelling regions[63]. UCYN-A2 was
343 also the dominant diazotroph, with comparable BNF rates to those in this study, peaking in
344 summer (ca. 2-3 nmol N L⁻¹d⁻¹) in both North Atlantic coastal waters[10] and the Subarctic

345 North Pacific[14]. However, there are at least three lines of evidence that point to an
346 unknown additional group of diazotrophs fixing N in this system. First, the relationship
347 between BNF magnitude and the abundance of UCYN-A reaches a plateau at rates above
348 $1 \text{ nmol N L}^{-1}\text{d}^{-1}$. Second, when the quantified *nifH* transcript copies L^{-1} are combined with
349 published cell-specific N_2 fixation rates for UCYN-A2 ($\sim 55 \text{ fmol N cell}^{-1} \text{ d}^{-1}$,[64]), the
350 calculated BNF magnitude is much lower than observed (Fig. S7). And lastly: at the
351 controlled conditions of the experimental nutrient additions, there are no relationship
352 between the change in BNF rates and the absolute abundance of *nifH* transcript copies L^{-1}
353 quantified by qPCR for UCYN-A2 (Fig. S8). Diatom-diazotroph associations (DDA)[65] were
354 not detected within our DNA/RNA sequencing. This absence might be surprising, as this
355 coastal upwelling region is dominated by diatoms during the spring-summer productive
356 season [36]. Several diatom genera that are host of diazotrophs (like *Hemiaulus* or
357 *Rhizosolenia*) are commonly present[66, 67], including in our samples[68]. Although the
358 non-detection of DDA N_2 -fixation activity aligns with previous size-fractionated incubations
359 that attributed BNF rates on the shelf off Ría de A Coruña exclusively to small
360 diazotrophs[20], it remains uncertain whether this absence of DDA contribution is due to a
361 methodological bias in the DNA amplification technique[69], or represents a true absence of
362 diazotroph symbionts. To disentangle the contribution of DDA versus UCYN-A in this region,
363 a closer visual inspection of the host cells, a DDA targeted nanoSIMS approach, and/or size-
364 fractionated incubations should be implemented in the future.

365 **Low N content and high temperature are the environmental drivers.**
366 Our results point out to temperature and low nitrogen content (evaluated through the N:P
367 ratio) as the environmental parameters that drive diazotroph community composition and
368 abundance in this coastal upwelling system. The relative enrichment of phosphorus as
369 compared to nitrogen confers a competitive advantage to diazotrophs since they are not
370 restricted by the nitrogen supply. This outcome, confirmed at community, taxa and ASV

371 level, is consistent with previous results. Temperature and N:P ratio have been identified as
372 the main controlling factors of diazotroph abundance in the North Pacific Ocean[27]. Warm
373 temperature ($>16^{\circ}\text{C}$) and lower NO_3^- content have been suggested as drivers of UCYN-A2
374 abundances in the California upwelling region[18]. Additionally, summer observations
375 carried out in the temperate western North Atlantic revealed that diazotroph community
376 composition and BNF correlated positively with *Chla* and P availability[9].

377 In addition, the short-term increase in PP and *Chla* observed in our nutrient amendment
378 experiments during summer and autumn, when low N:P ratio exists (Fig. 5A), indicates that
379 the phytoplankton standing stock was nitrogen-limited, or at least responsive to nitrogen
380 supply[70]. Interestingly, BNF rates were not completely prevented after NO_3^- addition in the
381 nutrient amendment experiments. A possible explanation for this is that UCYN-A2 lives in
382 symbiosis with a prymnesiophyte algae (*Braaudosphaera bigelowi*) exchanging fixed N for
383 fixed carbon[62, 71]. Indeed, the genome of UCYN-A is so streamlined to fuel BNF that it
384 even lacks genes for carbon fixation, oxygen-evolving photosystem II or nitrate assimilation
385 genes, so it is an obligate N_2 -fixer[72, 73], or even a new organelle[5]. Thus, UCYN-A
386 symbiosis relies on N_2 fixation even in N-rich environments[25]. It can be hypothesized that
387 the BNF decreases after nitrogen addition in our microcosms experiments not because of
388 inorganic nutrient inhibition, but due to the eukaryotic host algae being outcompeted by other
389 phytoplankton. Groups such as diatoms, characterized by high maximum nutrient uptake
390 and growth rates[74], may outcompete the slow growing *Braaudosphaera*/UCYN-A symbiosis
391 after nutrient additions[75], resulting in decreased BNF.

392 Puzzling out the diazotrophs niche

393 Then, how is the diazotroph niche constructed in this coastal upwelling region? We propose
394 a novel framework connecting hydrography and ecology through biogeochemical
395 processes. The full-depth biogeochemical sequence and its connection with surface BNF is

396 shown at a central station at the Ria de Vigo at weekly resolution for the period spring 2017
397 – spring 2018 (Fig. 6). Starting with hydrography, a key feature of this upwelling system is
398 the bidirectional exchange flow with a two-layer structure[76, 77]. During summer, when
399 upwelling conditions prevail, a positive circulation occurs in the Rías: cold subsurface water
400 enters through the lower layer (Fig. 6A), in contact with the bottom, while warm surface
401 waters flow out toward the shelf[39]. The upwelling causes the uplifting of the relatively
402 young Eastern North Atlantic Central Water (ENACW), which has an N:P ratio above or
403 close to one (Fig. 6B, , [29]), and low ammonium content ($\text{NH}_4 < 0.5 \mu\text{mol kg}^{-1}$, [78]).

404 Following with ecology, this region shows a rapid phytoplankton response to upwelling
405 pulses[40], as evidenced by the drawdown of inorganic nitrogen and the subsequent
406 chlorophyll accumulation (Fig. 6 B-D). After nitrogen drawdown through phytoplankton
407 uptake, a significant fraction of this fresh organic matter is remineralized within 1-2
408 weeks[78]. This recycling mechanism, also known as nutrient trapping, occurs when
409 particulate organic material sinks out of the photic zone but remains within the upwelling
410 system[78]. The signal of intense bottom remineralization that occurs over the shelf and
411 within the Rias is conveyed into the inner part of the bays, where nutrient trapping processes
412 magnifies, and then uplifts and exits in the surface outflow with the positive circulation[79].
413 The circulation outflow conveys a remineralization fingerprint that becomes more evident at
414 the surface as the upwelling-favorable season proceeds (Fig. 6B-C). This remineralization
415 fingerprint: (i) decreases the N:P ratio because P remineralization is quicker than that of
416 N[80–82], and (ii) accumulates ammonium regenerated within the Ria via ammonification
417 processes[83]. Evidence of cumulative remineralization is reflected in the seasonal evolution
418 of apparent oxygen utilization (AOU), a proxy for the net biological production or
419 consumption of oxygen, calculated as the difference between the observed dissolved
420 oxygen and its saturation concentration (Fig. 7). When AOU at the Ria de Vigo is assessed

421 with discrete samples of measured dissolved oxygen data from 1986-2018[84], it shows
422 lower negative values at the surface during spring and summer due to the oxygen production
423 linked to the synthesis of organic matter by autotrophs. Later, AOU reached its highest
424 positive values in deeper layers as oxygen was consumed during the breakdown of this
425 organic matter (Fig. 7).

426 We argue that in summer and early autumn, when BNF occurs, the signal from bottom
427 remineralization processes—following the sustained organic matter production during the
428 productive upwelling season—reaches the surface, conveyed by the positive circulation in
429 the Rías (sequential steps schematized in Fig. 8). This creates the optimum niche for BNF
430 in terms of temperature and inorganic nutrient content. The predominance of downwelling
431 conditions in late autumn/winter, which promote negative circulation in the Rías, combined
432 with low nutrient uptake by phytoplankton due to light limitation[29], and freshwater runoff
433 events reset the inorganic nutrient content in the surface layer to nitrogen replete conditions
434 (Fig. 6)[85], thereby disrupting the diazotroph niche and preventing BNF from occurring. It
435 is uncertain whether only an N:P ratio<1 is important, or the higher contribution of NH₄ over
436 NO₃⁻ to total inorganic nitrogen availability could also be a key factor in the formation of the
437 diazotroph niche. Higher temporal and spatial resolution data covering different
438 environmental conditions and/or multifactorial controlled experiments[86] are needed to
439 unravel the specific role of temperature and the contribution of NH₄.

440 The conceptual framework proposed in our study resembles the mechanistic niche
441 construction previously described in the eastern tropical North Atlantic Ocean [87], where
442 non-diazotrophs facilitate BNF by creating an environment with excess phosphate.
443 However, in our case, the trigger is the combination of predominant positive circulation within
444 the bays during the upwelling season, and the shorter turnover time of phosphorus
445 compared to nitrogen during organic matter remineralization [81]. The specific

446 characteristics of NW Iberia, such us the presence of elongated bays where upwelling is
447 relatively weak and intermittent[29], enable the ecological niche construction for diazotrophy.
448 Despite BNF representing a minor entry of new nitrogen into the euphotic zone compared
449 to other physical processes[20], it may be critical in supporting phytoplankton growth at the
450 end of the productive upwelling season. At this stage, the symbiosis between diatoms and
451 diazotrophs cyanobacteria could provide the necessary nitrogen to extend the productive
452 season further. Therefore, these results could help explain why the upwelling bays are more
453 productive compared to the upwelled offshore waters[32]. Future studies are needed to
454 investigate the specific role of diatom-diazotroph associations in the productivity of the
455 upwelling bays, and the extent to which similar processes occur in other coastal upwelling
456 regions.

457

458 References

- 459 1. Gruber N, Galloway JN. An Earth-system perspective of the global nitrogen cycle. *Nature*
460 2008; **451**: 293–296.
- 461 2. Zehr JP, Capone DG. Changing perspectives in marine nitrogen fixation. *Science* 2020; **368**:
462 eaay9514.
- 463 3. Turk-Kubo KA, Gradoville MR, Cheung S, Cornejo-Castillo FM, Harding KJ, Morando M, et al.
464 Non-cyanobacterial diazotrophs: global diversity, distribution, ecophysiology, and activity in
465 marine waters. *FEMS Microbiology Reviews* 2023; **47**: fuac046.
- 466 4. Martínez-Pérez C, Mohr W, Löscher CR, Dekaezemacker J, Littmann S, Yilmaz P, et al. The
467 small unicellular diazotrophic symbiont, UCYN-A, is a key player in the marine nitrogen cycle.
468 *Nature Microbiology* 2016; **1**: 16163.

- 469 5. Coale TH, Loconte V, Turk-Kubo KA, Vanslembrouck B, Mak WKE, Cheung S, et al. Nitrogen-
470 fixing organelle in a marine alga. *Science* 2024; **384**: 217–222.
- 471 6. Knapp A. The sensitivity of marine N₂ fixation to dissolved inorganic nitrogen. *Frontiers in*
472 *Microbiology* 2012; **3**.
- 473 7. Li D, Jing H, Zhang R, Yang W, Chen M, Wang B, et al. Heterotrophic diazotrophs in a
474 eutrophic temperate bay (Jiaozhou Bay) broadens the domain of N₂ fixation in China's
475 coastal waters. *Estuarine, Coastal and Shelf Science* 2020; **242**: 106778.
- 476 8. Selden CR, Chappell PD, Clayton S, Macías-Tapia A, Bernhardt PW, Mulholland MR. A coastal
477 N fixation hotspot at the Cape Hatteras front: Elucidating spatial heterogeneity in diazotroph
478 activity via supervised machine learning. *Limnology and Oceanography* 2021; **66**: 1832–1849.
- 479 9. Tang W, Wang S, Fonseca-Batista D, Dehairs F, Gifford S, Gonzalez AG, et al. Revisiting the
480 distribution of oceanic N₂ fixation and estimating diazotrophic contribution to marine
481 production. *Nature Communications* 2019; **10**: 831.
- 482 10. Tang W, Cerdán-García E, Berthelot H, Polyviou D, Wang S, Baylay A, et al. New insights into
483 the distributions of nitrogen fixation and diazotrophs revealed by high-resolution sensing
484 and sampling methods. *The ISME Journal* 2020; **14**: 2514–2526.
- 485 11. Harding K, Turk-Kubo KA, Sipler RE, Mills MM, Bronk DA, Zehr JP. Symbiotic unicellular
486 cyanobacteria fix nitrogen in the Arctic Ocean. *Proceedings of the National Academy of*
487 *Sciences* 2018; **115**: 13371–13375.
- 488 12. Raes EJ, van de Kamp J, Bodrossy L, Fong AA, Riekenberg J, Holmes BH, et al. N₂ Fixation and
489 New Insights Into Nitrification From the Ice-Edge to the Equator in the South Pacific Ocean.
490 *Frontiers in Marine Science* 2020; **7**.

- 491 13. Sato T, Shiozaki T, Taniuchi Y, Kasai H, Takahashi K. Nitrogen Fixation and Diazotroph
492 Community in the Subarctic Sea of Japan and Sea of Okhotsk. *Journal of Geophysical*
493 *Research: Oceans* 2021; **126**: e2020JC017071.
- 494 14. Shiozaki T, Bombar D, Riemann L, Hashihama F, Takeda S, Yamaguchi T, et al. Basin scale
495 variability of active diazotrophs and nitrogen fixation in the North Pacific, from the tropics to
496 the subarctic Bering Sea. *Global Biogeochemical Cycles* 2017; **31**: 996–1009.
- 497 15. Bentzon-Tilia M, Traving SJ, Mantikci M, Knudsen-Leerbeck H, Hansen JLS, Markager S, et al.
498 Significant N₂ fixation by heterotrophs, photoheterotrophs and heterocystous cyanobacteria
499 in two temperate estuaries. *The ISME Journal* 2015; **9**: 273–285.
- 500 16. Hallstrøm S, Benavides M, Salamon ER, Arístegui J, Riemann L. Activity and distribution of
501 diazotrophic communities across the Cape Verde Frontal Zone in the Northeast Atlantic
502 Ocean. *Biogeochemistry* 2022; **160**: 49–67.
- 503 17. Mulholland MR, Bernhardt PW, Widner BN, Selden CR, Chappell PD, Clayton S, et al. High
504 Rates of N₂ Fixation in Temperate, Western North Atlantic Coastal Waters Expand the Realm
505 of Marine Diazotrophy. *Global Biogeochemical Cycles* 2019; **33**: 826–840.
- 506 18. Cabello AM, Turk-Kubo KA, Hayashi K, Jacobs L, Kudela RM, Zehr JP. Unexpected presence of
507 the nitrogen-fixing symbiotic cyanobacterium UCYN-A in Monterey Bay, California. *Journal of*
508 *Phycology* 2020; **56**: 1521–1533.
- 509 19. Moreira-Coello V, Mouriño-Carballedo B, Marañón E, Fernández-Carrera A, Bode A, Sintes E,
510 et al. Temporal variability of diazotroph community composition in the upwelling region off
511 NW Iberia. *Scientific Reports* 2019; **9**: 3737.
- 512 20. Moreira-Coello V, Mouriño-Carballedo B, Marañón E, Fernández-Carrera A, Bode A, Varela
513 MM. Biological N₂ Fixation in the Upwelling Region off NW Iberia: Magnitude, Relevance,
514 and Players. *Frontiers in Marine Science* 2017; **4**.

- 515 21. Benavides M, Shoemaker KM, Moisander PH, Niggemann J, Dittmar T, Duhamel S, et al.
- 516 Aphotic N₂ fixation along an oligotrophic to ultraoligotrophic transect in the western tropical
- 517 South Pacific Ocean. *Biogeosciences* 2018; **15**: 3107–3119.
- 518 22. Ward BA, Dutkiewicz S, Moore CM, Follows MJ. Iron, phosphorus, and nitrogen supply ratios
- 519 define the biogeography of nitrogen fixation. *Limnology and Oceanography* 2013; **58**: 2059–
- 520 2075.
- 521 23. Tang W, Cassar N. Data-Driven Modeling of the Distribution of Diazotrophs in the Global
- 522 Ocean. *Geophysical Research Letters* 2019; **46**: 12258–12269.
- 523 24. Langlois RJ, Mills MM, Ridame C, Croot P, LaRoche J. Diazotrophic bacteria respond to
- 524 Saharan dust additions. *Mar Ecol Prog Ser* 2012; **470**: 1–14.
- 525 25. Mills MM, Turk-Kubo KA, van Dijken GL, Henke BA, Harding K, Wilson ST, et al. Unusual
- 526 marine cyanobacteria/haptophyte symbiosis relies on N₂ fixation even in N-rich
- 527 environments. *The ISME Journal* 2020; **14**: 2395–2406.
- 528 26. Villamaña M, Marañón E, Cermeño P, Estrada M, Fernández-Castro B, Figueiras FG, et al. The
- 529 role of mixing in controlling resource availability and phytoplankton community composition.
- 530 *Progress in Oceanography* 2019; **178**: 102181.
- 531 27. Cheung S, Nitanai R, Tsurumoto C, Endo H, Nakaoka S, Cheah W, et al. Physical Forcing
- 532 Controls the Basin-Scale Occurrence of Nitrogen-Fixing Organisms in the North Pacific Ocean.
- 533 *Global Biogeochemical Cycles* 2020; **34**: e2019GB006452.
- 534 28. Arístegui J, Barton ED, Álvarez-Salgado XA, Santos AMP, Figueiras FG, Kifani S, et al. Sub-
- 535 regional ecosystem variability in the Canary Current upwelling. *Progress in Oceanography*
- 536 2009; **83**: 33–48.

- 537 29. Castro CG, Pérez FF, Álvarez-Salgado XA, Fraga F. Coupling between the thermohaline,
538 chemical and biological fields during two contrasting upwelling events off the NW Iberian
539 Peninsula. *Continental Shelf Research* 2000; **20**: 189–210.
- 540 30. Fraga F. Upwelling off the Galician Coast, Northwest Spain. In: Richards FA (ed). *Coastal*
541 *Upwelling*. 1981. American Geophysical Union, pp 176–182.
- 542 31. Wooster WS, Bakun A, McLain DR. SEASONAL UPWELLING CYCLE ALONG THE EASTERN
543 BOUNDARY OF THE NORTH ATLANTIC. *Journal of Marine Research* 1976; **34**: 131–141.
- 544 32. Largier JL. Upwelling Bays: How Coastal Upwelling Controls Circulation, Habitat, and
545 Productivity in Bays. *Annual Review of Marine Science* 2020; **12**: 415–447.
- 546 33. Garza-Gil MD, Surís-Regueiro JC, Varela-Lafuente MM. Using input–output methods to assess
547 the effects of fishing and aquaculture on a regional economy: The case of Galicia, Spain.
548 *Marine Policy* 2017; **85**: 48–53.
- 549 34. Figueiras FG, Teixeira IG, Froján M, Zúñiga D, Arbones B, Castro CG. Seasonal Variability in
550 the Microbial Plankton Community in a Semienclosed Bay Affected by Upwelling: The Role of
551 a Nutrient Trap. *Front Mar Sci* 2020; **7**.
- 552 35. Figueiras FG, Ríos AF. Phytoplankton succession, red tides and the hydrographic regime in
553 the Rias Bajas of Galicia. In: Smayda TJ, Shimizu Y (eds). *Toxic Phytoplankton Blooms in the*
554 *Sea*. 1993. Elsevier, New York, USA, pp 239–244.
- 555 36. Cermeño P, Marañón E, Pérez V, Serret P, Fernández E, Castro CG. Phytoplankton size
556 structure and primary production in a highly dynamic coastal ecosystem (Ría de Vigo, NW-
557 Spain): Seasonal and short-time scale variability. *Estuarine, Coastal and Shelf Science* 2006;
558 **67**: 251–266.

- 559 37. Agawin NSR, Benavides M, Busquets A, Ferriol P, Stal LJ, Arístegui J. Dominance of unicellular
560 cyanobacteria in the diazotrophic community in the Atlantic Ocean. *Limnology and*
561 *Oceanography* 2014; **59**: 623–637.
- 562 38. Benavides M, Agawin NSR, Arístegui J, Ferriol P, Stal LJ. Nitrogen fixation by Trichodesmium
563 and small -diazotrophs in the subtropical northeast Atlantic. *Aquat Microb Ecol* 2011; **65**: 43–
564 53.
- 565 39. Comesaña A, Fernández-Castro B, Chouciño P, Fernández E, Fuentes-Lema A, Gilcoto M, et
566 al. Mixing and Phytoplankton Growth in an Upwelling System. *Frontiers in Marine Science*
567 2021; **8**.
- 568 40. Broullón E, Franks PJS, Fernández Castro B, Gilcoto M, Fuentes-Lema A, Pérez-Lorenzo M, et
569 al. Rapid phytoplankton response to wind forcing influences productivity in upwelling bays.
570 *Limnology and Oceanography Letters* 2023; **8**: 529–537.
- 571 41. Hansen HP, Koroleff F. Determination of nutrients. *Methods of Seawater Analysis*. 1999. pp
572 159–228.
- 573 42. Kérouel R, Aminot A. Fluorometric determination of ammonia in sea and estuarine waters by
574 direct segmented flow analysis. *Marine Chemistry* 1997; **57**: 265–275.
- 575 43. Prandke H, Stips A. Test measurements with an operational microstructure-turbulence
576 profiler: Detection limit of dissipation rates. *Aquat Sci* 1998; **60**: 191–209.
- 577 44. Deutsch C, Weber T. Nutrient Ratios as a Tracer and Driver of Ocean Biogeochemistry.
578 *Annual Review of Marine Science* . 2012. Annual Reviews. , **4**: 113–141
- 579 45. Montoya JP, Voss M, Kahler P, Capone DG. A Simple, High-Precision, High-Sensitivity Tracer
580 Assay for N($\text{inf}2$) Fixation. *Applied and Environmental Microbiology* 1996; **62**: 986–993.

- 581 46. White AE, Granger J, Selden C, Gradoville MR, Potts L, Bourbonnais A, et al. A critical review
582 of the $^{15}\text{N}_2$ tracer method to measure diazotrophic production in pelagic ecosystems.
- 583 *Limnology and Oceanography: Methods* 2020; **18**: 129–147.
- 584 47. Zehr JP, McReynolds LA. Use of degenerate oligonucleotides for amplification of the nifH
585 gene from the marine cyanobacterium *Trichodesmium thiebautii*. *Applied and Environmental
586 Microbiology* 1989; **55**: 2522–2526.
- 587 48. Zehr JP, Turner PJ. Nitrogen fixation: Nitrogenase genes and gene expression. *Methods in
588 Microbiology*. 2001. Academic Press, pp 271–286.
- 589 49. Thompson A, Carter BJ, Turk-Kubo K, Malfatti F, Azam F, Zehr JP. Genetic diversity of the
590 unicellular nitrogen-fixing cyanobacteria UCYN-A and its prymnesiophyte host.
- 591 *Environmental Microbiology* 2014; **16**: 3238–3249.
- 592 50. Church MJ, Jenkins BD, Karl DM, Zehr JP. Vertical distributions of nitrogen-fixing phylotypes
593 at Stn Aloha in the oligotrophic North Pacific Ocean. *Aquatic Microbial Ecology* 2005; **38**: 3–
594 14.
- 595 51. Moisander PH, Beinart RA, Voss M, Zehr JP. Diversity and abundance of diazotrophic
596 microorganisms in the South China Sea during intermonsoon. *ISME J* 2008; **2**: 954–967.
- 597 52. Callahan BJ, McMurdie PJ, Rosen MJ, Han AW, Johnson AJA, Holmes SP. DADA2: High-
598 resolution sample inference from Illumina amplicon data. *Nat Methods* 2016; **13**: 581–583.
- 599 53. Angel R, Nepel M, Panholzl C, Schmidt H, Herbold CW, Eichorst SA, et al. Evaluation of
600 Primers Targeting the Diazotroph Functional Gene and Development of NifMAP – A
601 Bioinformatics Pipeline for Analyzing nifH Amplicon Data. *Front Microbiol* 2018; **9**.
- 602 54. Zehr JP, Jenkins BD, Short SM, Steward GF. Nitrogenase gene diversity and microbial
603 community structure: a cross-system comparison. *Environmental Microbiology* 2003; **5**: 539–
604 554.

- 605 55. Camacho C, Coulouris G, Avagyan V, Ma N, Papadopoulos J, Bealer K, et al. BLAST+:
606 architecture and applications. *BMC Bioinformatics* 2009; **10**: 421.
- 607 56. Heller P, Tripp HJ, Turk-Kubo K, Zehr JP. ARBitrator: a software pipeline for on-demand
608 retrieval of auto-curated nifH sequences from GenBank. *Bioinformatics* 2014; **30**: 2883–
609 2890.
- 610 57. Oksanen J, Simpson GL, Blanchet FG, Kindt R, Legendre P, Minchin PR, et al. vegan:
611 Community Ecology Package. 2024.
- 612 58. Mouillot D, Stubbs W, Faure M, Dumay O, Tomasini JA, Wilson JB, et al. Niche Overlap
613 Estimates Based on Quantitative Functional Traits: A New Family of Non-Parametric Indices.
614 *Oecologia* 2005; **145**: 345–353.
- 615 59. Geange SW, Pledger S, Burns KC, Shima JS. A unified analysis of niche overlap incorporating
616 data of different types. *Methods in Ecology and Evolution* 2011; **2**: 175–184.
- 617 60. Martin BD, Witten D, Willis AD. Modeling microbial abundances and dysbiosis with beta-
618 binomial regression. *The Annals of Applied Statistics* 2020; **14**: 94–115.
- 619 61. Turk-Kubo KA, Mills MM, Arrigo KR, van Dijken G, Henke BA, Stewart B, et al. UCYN-
620 A/haptophyte symbioses dominate N2 fixation in the Southern California Current System.
621 *ISME COMMUN* 2021; **1**: 1–13.
- 622 62. Zehr JP, Shilova IN, Farnelid HM, Muñoz-Marín M del C, Turk-Kubo KA. Unusual marine
623 unicellular symbiosis with the nitrogen-fixing cyanobacterium UCYN-A. *Nat Microbiol* 2016;
624 **2**: 1–11.
- 625 63. Selden CR, Mulholland MR, Crider KE, Clayton S, Macías-Tapia A, Bernhardt P, et al. Nitrogen
626 Fixation at the Mid-Atlantic Bight Shelfbreak and Transport of Newly Fixed Nitrogen to the
627 Slope Sea. *Journal of Geophysical Research: Oceans* 2024; **129**: e2023JC020651.

- 628 64. Shao Z, Xu Y, Wang H, Luo W, Wang L, Huang Y, et al. Global oceanic diazotroph database
629 version 2 and elevated estimate of global oceanic N₂ fixation. *Earth System Science Data*
630 2023; **15**: 3673–3709.
- 631 65. Foster RA, Zehr JP. Characterization of diatom–cyanobacteria symbioses on the basis of nifH,
632 hetR and 16S rRNA sequences. *Environmental Microbiology* 2006; **8**: 1913–1925.
- 633 66. Estrada M. Phytoplankton distribution and composition off the coast of Galicia (northwest of
634 Spain). *Journal of Plankton Research* 1984; **6**: 417–434.
- 635 67. Ospina-Alvarez N, Varela M, Doval MD, Gómez-Gesteira M, Cervantes-Duarte R, Prego R.
636 Outside the paradigm of upwelling rias in NW Iberian Peninsula: Biogeochemical and
637 phytoplankton patterns of a non-upwelling ria. *Estuarine, Coastal and Shelf Science* 2014;
638 **138**: 1–13.
- 639 68. Velasco-Senovilla E, Reguera B, Ramilo I, Casas G, Mouríño-Carballedo B, Nogueira E.
640 Upwelling events, depth varying succession of phytoplankton assemblages and vertical
641 connectivity: a conceptual model. *in prep* 2025.
- 642 69. Farnelid H, Turk-Kubo K, Muñoz-Marín M del C, Zehr JP. New insights into the ecology of the
643 globally significant uncultured nitrogen-fixing symbiont UCYN-A. *Aquatic Microbial Ecology*
644 2016; **77**: 125–138.
- 645 70. Martínez-García S, Fernández E, Álvarez-Salgado X-A, González J, Lønborg C, Marañón E, et
646 al. Differential responses of phytoplankton and heterotrophic bacteria to organic and
647 inorganic nutrient additions in coastal waters off the NW Iberian Peninsula. *Marine Ecology
648 Progress Series* 2010; **416**: 17–33.
- 649 71. Hagino K, Onuma R, Kawachi M, Horiguchi T. Discovery of an Endosymbiotic Nitrogen-Fixing
650 Cyanobacterium UCYN-A in *Braarudosphaera bigelowii* (Prymnesiophyceae). *PLOS ONE* 2013;
651 **8**: e81749.

- 652 72. Cornejo-Castillo FM, Cabello AM, Salazar G, Sánchez-Baracaldo P, Lima-Mendez G, Hingamp
653 P, et al. Cyanobacterial symbionts diverged in the late Cretaceous towards lineage-specific
654 nitrogen fixation factories in single-celled phytoplankton. *Nat Commun* 2016; **7**: 11071.
- 655 73. Tripp HJ, Bench SR, Turk KA, Foster RA, Desany BA, Niazi F, et al. Metabolic streamlining in an
656 open-ocean nitrogen-fixing cyanobacterium. *Nature* 2010; **464**: 90–94.
- 657 74. Sommer U. The paradox of the plankton: Fluctuations of phosphorus availability maintain
658 diversity of phytoplankton in flow-through cultures. *Limnology and Oceanography* 1984; **29**:
659 633–636.
- 660 75. Teira E, Martínez-García S, Carreira C, Morán X-AG. Changes in bacterioplankton and
661 phytoplankton community composition in response to nutrient additions in coastal waters
662 off the NW Iberian Peninsula. *Marine Ecology Progress Series* 2011; **426**: 87–104.
- 663 76. Gilcoto M, Largier JL, Barton ED, Piedracoba S, Torres R, Graña R, et al. Rapid response to
664 coastal upwelling in a semienclosed bay. *Geophysical Research Letters* 2017; **44**: 2388–2397.
- 665 77. Souto C, Gilcoto M, Fariña-Busto L, Pérez FizF. Modeling the residual circulation of a coastal
666 embayment affected by wind-driven upwelling: Circulation of the Ría de Vigo (NW Spain).
667 *Journal of Geophysical Research: Oceans* 2003; **108**.
- 668 78. Álvarez-Salgado XA, Castro CG, Pérez FF, Fraga F. Nutrient mineralization patterns in shelf
669 waters of the Western Iberian upwelling. *Continental Shelf Research* 1997; **17**: 1247–1270.
- 670 79. Rosón G, Álvarez-Salgado XA, Pérez FF. Carbon cycling in a large coastal embayment,
671 affected by wind-driven upwelling: short-time-scale variability and spatial differences.
672 *Marine Ecology Progress Series* 1999; **176**: 215–230.
- 673 80. Garber JH. Laboratory study of nitrogen and phosphorus remineralization during the
674 decomposition of coastal plankton and seston. *Estuarine, Coastal and Shelf Science* 1984; **18**:
675 685–702.

- 676 81. Nogueira E, Pérez FF, Ríos AF. Seasonal Patterns and Long-term Trends in an Estuarine
677 Upwelling Ecosystem (Ría de Vigo, NW Spain). *Estuarine, Coastal and Shelf Science* 1997; **44**:
678 285–300.
- 679 82. Pérez FF, Ríos AF, Rellán T, Alvarez M. Improvements in a fast potentiometric seawater
680 alkalinity determination. *Ciencias Marinas* 2000; **26**: 463–478.
- 681 83. Alonso-Pérez F, Castro CG. Benthic oxygen and nutrient fluxes in a coastal upwelling system
682 (Ria de Vigo, NW Iberian Peninsula): seasonal trends and regulating factors. *Marine Ecology
683 Progress Series* 2014; **511**: 17–32.
- 684 84. Padin XA, Velo A, Pérez FF. ARIOS: a database for ocean acidification assessment in the
685 Iberian upwelling system (1976–2018). *Earth System Science Data* 2020; **12**: 2647–2663.
- 686 85. Álvarez-Salgado XA, Borges A, Figueiras FG, Chou L. Iberian margin: the Rías. *Carbon and
687 Nutrient Fluxes in Continental Margins* 2010; 102–119.
- 688 86. Marañón E, Cermeño P, Huete-Ortega M, López-Sandoval DC, Mouriño-Carballido B,
689 Rodríguez-Ramos T. Resource Supply Overrides Temperature as a Controlling Factor of
690 Marine Phytoplankton Growth. *PLOS ONE* 2014; **9**: e99312.
- 691 87. Singh A, Bach LT, Fischer T, Hauss H, Kiko R, Paul AJ, et al. Niche construction by non-
692 diazotrophs for N₂ fixers in the eastern tropical North Atlantic Ocean. *Geophysical Research
693 Letters* 2017; **44**: 6904–6913.
- 694

695 **Figure legends**

696 **Figure 1. Diazotrophic abundance and community composition, and biological**
697 **nitrogen fixation.** Temporal variability of **A)** *nifH* amplicon-based sequencing community
698 composition (relative abundance %) for the most abundant taxa, ordered from top to bottom
699 in increasing abundance. Blank gaps are discarded samples due DNA extraction issues or
700 unacceptable rarefaction curves. **B)** Nitrogen fixation rate ($\text{nmol N L}^{-1}\text{d}^{-1}$) measurements.
701 When values were below detection limits, they are represented with a red border. Error bars
702 represents triplicate measurements (if not visible, they are not larger than the dots). Note
703 the square root transformation on the y-axis (not linear to help in the visualization of small
704 values). **C)** quantitative *nifH* gene copy abundance (qPCR, *nifH* gene copies L^{-1}) data for
705 UCYN-A2, UCYN-A1 and *Gammaproteobacteria* 24774A11. Note that the color scale is
706 logarithmic. UCYN-A2 abundance on 22nd June 2017 exceeded the scale's range by an
707 order of magnitude ($1.7 \pm 0.7 \times 10^6 \text{ nifH transcripts copies} \cdot \text{L}^{-1}$), and it was replaced by a black
708 triangle for visualization purposes. The same figure without this visual solution can be seen
709 in Fig. S6. Climatological season is represented in the inner colored band. The x-axis is
710 shared for the three graphs, sampling dates (format: year/month/day) colored according to
711 location (color code for the locations in Fig. S1). Times when nitrogen amendment
712 experiments were performed are indicated with orange crosses in the upper margin of B).

713

714 **Figure 2. UCYN-A *nifH* gene abundance and expression.** Relationship between BNF
715 ($\text{nmol N L}^{-1}\text{d}^{-1}$) and the abundance of UCYN-A ecotypes (A1 and A2). Quantification of *nifH*
716 gene copies/L by qPCR from DNA (circles) and *nifH* gene transcripts/L by RT-qPCR from
717 cDNA (triangles). Note that the y-scale is logarithmic. Error bars in the y-axis represent
718 standard deviation from three replicates per sample (if not visible, they are not larger than
719 the dots). Uncertainty in N_2 -fixation rates is represented in the x-axis with gray horizontal

720 bars spanning the triplicates measurements (only for UCYN-A2). Samples with positive BNF
721 and non-detection by qPCR are included on the x-axis with red bordering.

722 **Figure 3. Taxa dominance is related with environmental conditions.** Principal
723 Coordinates Analysis (PCoA) based on Bray-Curtis dissimilarity matrix illustrating the
724 differences between samples dominated by UCYN-A (cyan circles) and non-cyanobacterial
725 diazotrophs (NCD, orange squares). Sample group centroids for each dominance situation
726 and confidence ellipses displaying the standard deviation of centroid locations are also
727 represented. The environmental factors (%NH₄, N:P ratio, in situ temperature, NO₃⁻ and
728 PO₄) that contributed most to the community differences observed between these
729 dominance situations were fitted through significant ($p < 0.001$) vector overlays (black color)
730 onto the PCoA ordination. The first axis of the PCoA (x-axis) explains 29.4% of the variance,
731 and the second axis (y-axis) 5.1%.

732 **Figure 4. Temperature and inorganic nitrogen conditions are niche descriptors of the**
733 **diazotrophic community.** A) Kernel density estimates for the taxonomical groups and the
734 niche descriptors inorganic nutrient content, (N:P ratio, A; % of NH₄ in total DIN, B) and
735 temperature (°C, C) separated by cyanobacterial (cyan) and non-cyanobacterial diazotrophs
736 (orange). The red vertical line in A) at N:P ratio=1 delimits apparent nitrogen limitation
737 conditions (when the ratio is <1, left side of the graph). Deviations from N:P ratio=1 (red
738 dashed line in Fig. 4A) separate conditions when there is phosphorus in excess (on the left
739 side of the plot) from conditions of nitrogen surplus (on the right side). The y-axis represents
740 the probability density function for the kernel density estimation. B) Coefficients of models
741 after beta-binomial regression for the environmental parameters inorganic nutrient content
742 (N:P ratio, left column; % of NH₄ in total DIN, mid) and temperature (right column). Only
743 significant models ($p \leq 0.05$) from the whole diazotroph community (7030 ASVs) are shown.
744 The coefficient estimate indicates positive or negative responses to the parameter and is

745 shown with a 95% confidence interval. Specie identification in the y-axis label is only shown
746 when BLASTp result is >=95% (percentage in parentheses). For these ASVs, a detailed
747 table with taxonomy info and complete *nifH* sequence is available as supporting info table.
748 The color code is shared at taxa level for both panels.

749 **Figure 5. Biological nitrogen fixation (BNF) decreases with inorganic nitrogen**
750 **additions when the plankton community is N-limited.** Response of BNF, primary
751 production rates and *chl a* after nutrient amendment microcosm experiments through each
752 climatological season (n= 4) **A)** BNF (nmol N L⁻¹d⁻¹) at in situ conditions (natural
753 environment), inside the microcosm setting ("Control") and the response after 24 hours in
754 the nitrate (+NO₃⁻) or ammonia (+NH₄) amendment treatments. Red dashed horizontal line
755 represents the methodological limit of detection for each triplicate of measurements (black
756 dots). **B)** Response ratio defined as the change in absolute value with regard to initial
757 conditions after 24 hours for N₂-fixation, and after 72 hours for *Chl a* and/or Primary
758 Production (PP). Values below 1 (red dashed line) are mean reductions and values above
759 1 mean increases.

760 **Figure 6. Hydrographic full-depth variability at weekly resolution at the central Ria de**
761 **Vigo during spring 2017 – spring 2018.** Time-series of the full-depth vertical distribution
762 of A) temperature (°C). The white solid line represents the isotherm of 16 °C. B) N:P ratio.
763 The green and black solid line represents the isoline of 0.45 and 1, respectively. C) % of
764 NH₄ in DIN. The white solid line represents the isoline of 75%. And D) Chlorophyll a (Chl a)
765 concentration (mg·m⁻³). Dots represent sample vertical resolution. Surface black circles
766 represents nitrogen fixation rate measurements. When values were below detection limits,
767 they are represented with a red border. Climatological season is represented in the top
768 colored band. The hydrographic conditions with respect to upwelling (blue), downwelling
769 (red), and transition (gray) in the low colored band following[39].

770 **Figure 7. Annual variability of apparent oxygen utilization (AOU, $\mu\text{mol kg}^{-1}$), a proxy of**
771 **the biological production and consumption of oxygen, at the Ria de Vigo.** It includes
772 discrete samples of measured dissolved oxygen data from 1986-2018[84] and the shelf/Ría
773 separation criteria (panels left and right) was considered at 9°W longitude (westernmost
774 location 9.5°W). Depth bands grouped each 10 m, from surface (0 m) to bottom (40 m,
775 maximum depth of central Ria de Vigo station) have been modelled with a locally weighted
776 polynomial regression (LOESS). Oversaturation of oxygen due biological production (AOU
777 $<0, \mu\text{mol kg}^{-1}$) and undersaturation due respiration (AOU $>0, \mu\text{mol kg}^{-1}$) are separated by
778 the red-dashed line. The vertical solid lines represent the onset of climatological seasons.

779 **Figure 8. The sequential steps of the mechanistic biogeochemical niche construction**
780 **process for nitrogen fixers.** (A) At the beginning of the upwelling season, sea surface
781 temperature (SST) is still cold. Upwelled ENACW brings nutrients upwards, into the ría,
782 sustaining an elevated N:P ratio and low content in the form of NH_4^+ . (B) Phytoplankton grow
783 within the surface layer due to the previous nutrient input and the necessary irradiance.
784 Subsequently, (C) organic matter produced by phytoplankton is exported to the outer part
785 of the ría, where it sinks. (D) This organic matter is remineralized near the bottom, where P
786 content rapidly increases, lowering N:P levels. There, inorganic nitrogen is mostly in the form
787 of NH_4^+ . (E) Further into the upwelling season, upwelled waters are mixed with the
788 remineralized P-rich waters, and positive upwelling circulation transports them towards the
789 surface. (F) At the end of the summer upwelling season, SST has increased ($> 16^\circ\text{C}$) and
790 nitrogen fixers can take an advantage of it, in combination to the low N:P conditions.

791

792 Acknowledgements

793 MF was funded by Juan de La Cierva Formación (FJC2019-038970-I, Ministerio de Ciencia
794 e Innovación, Spanish Government). Additional funds for molecular analysis were coming
795 from Axencia Galega de Innovacion (agreement GAIN-IEO) and GRC-EPB Plankton
796 Ecology and Biogeochemistry Research Group (ref. IN607A2018/2). This research was
797 funded by project REMEDIOS (CTM2016-75451-C2-1-R) to BM-C from the Spanish Ministry
798 of Economy and Competitiveness. Bioinformatic analysis were partially run at the Centro de
799 Supercomputación de Galicia (CESGA). We thank E. Teira, E. Fernández, A. Fuentes, M.
800 Pérez, E. Peláez and S. Vieitez, M. J. Pazó, V. Vieitez, C. Rodríguez, J. Valencia, R. Alba-
801 Salgueiro for their assistance during field experiments and lab analysis. We thank X. A.
802 Álvarez-Salgado for her helpful comments on an early version of the draft.

803

804 Data Availability Statement

805 Source datasets supporting the current study are available in
806 https://figshare.com/collections/Mixing_and_Phytoplankton_Growth_in_an_Upwelling_System/5604209 and <https://data.mendeley.com/datasets/pm4r2pyy3/2>. *nifH* sequences are
807 deposited in SRA with accession number PRJNA1184991
808 <https://www.ncbi.nlm.nih.gov/bioproject/PRJNA1184991>. Code and data to reproduce the
809 results is publicly available in https://github.com/mfontela/nifH_niche

811

812

Figure 1

Click here to access/download;Figure;Figure1.pdf

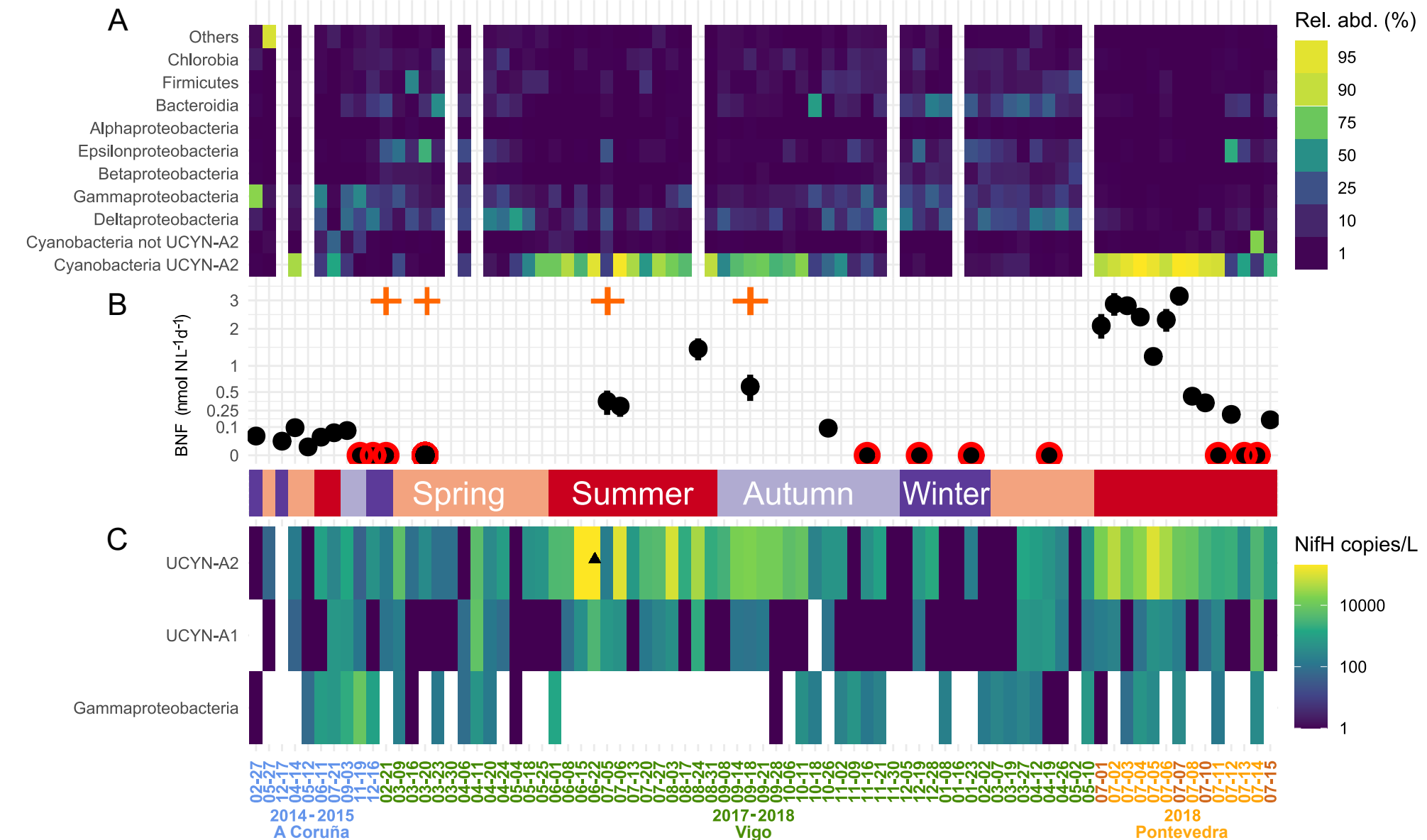


Figure 2

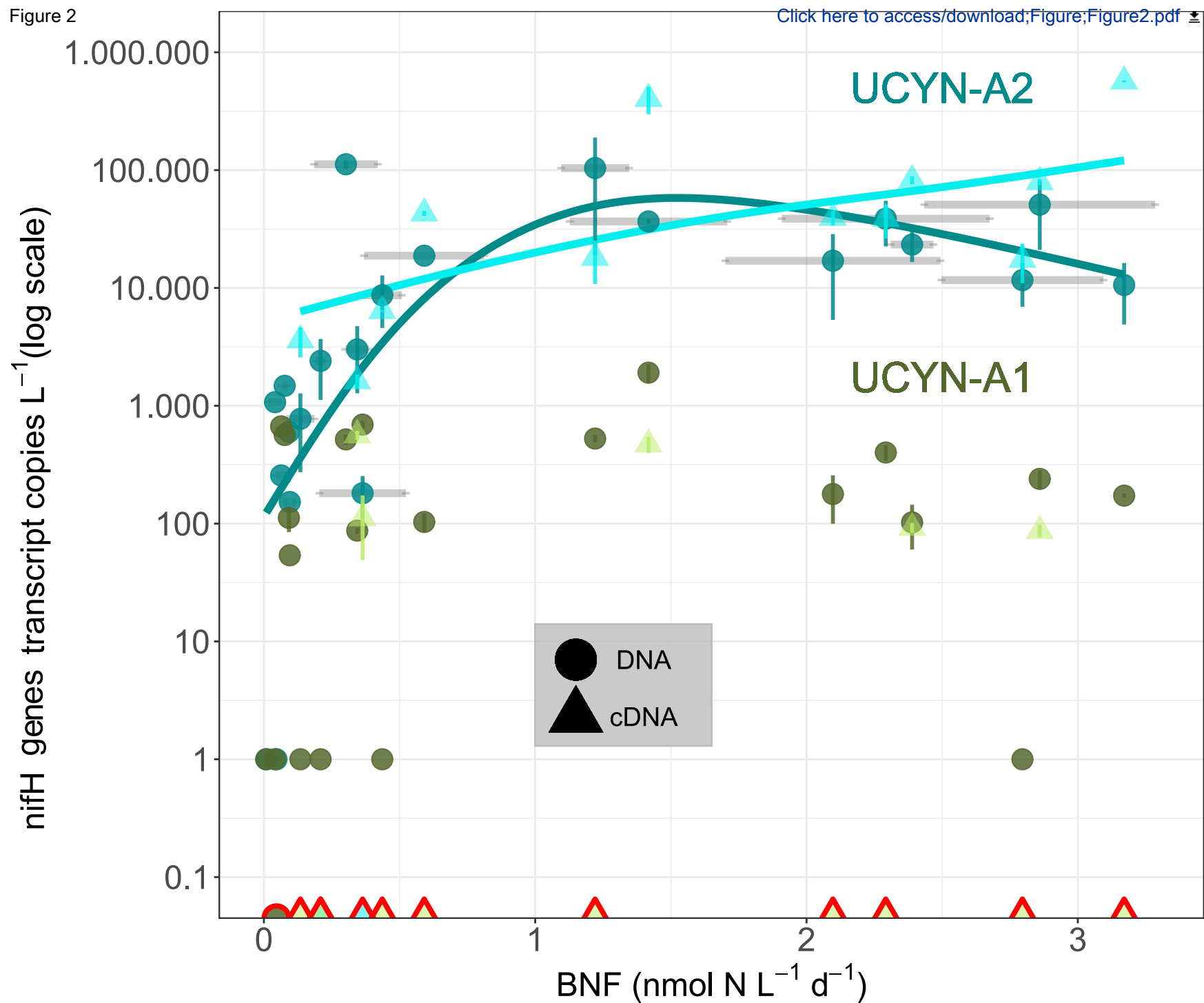
[Click here to access/download;Figure;Figure2.pdf](#)

Figure 3

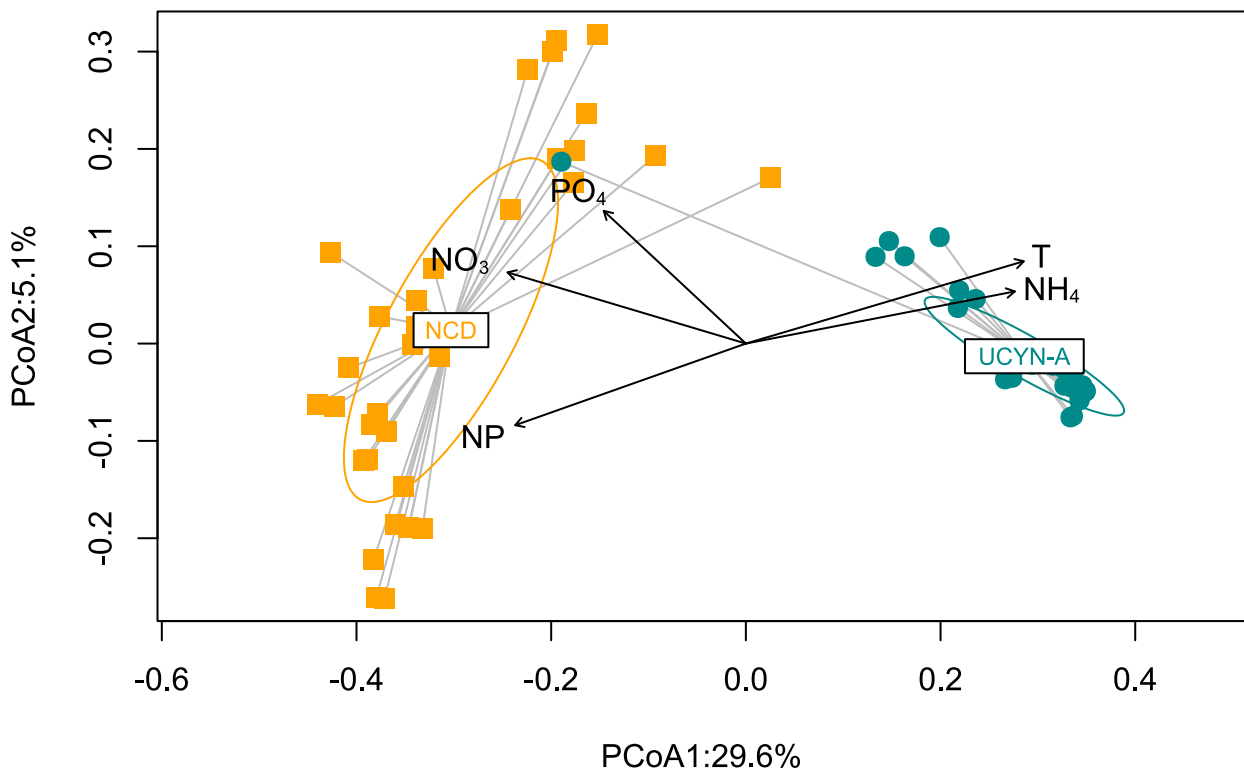
[Click here to access/download;Figure;Figure3.pdf](#)

Figure 4

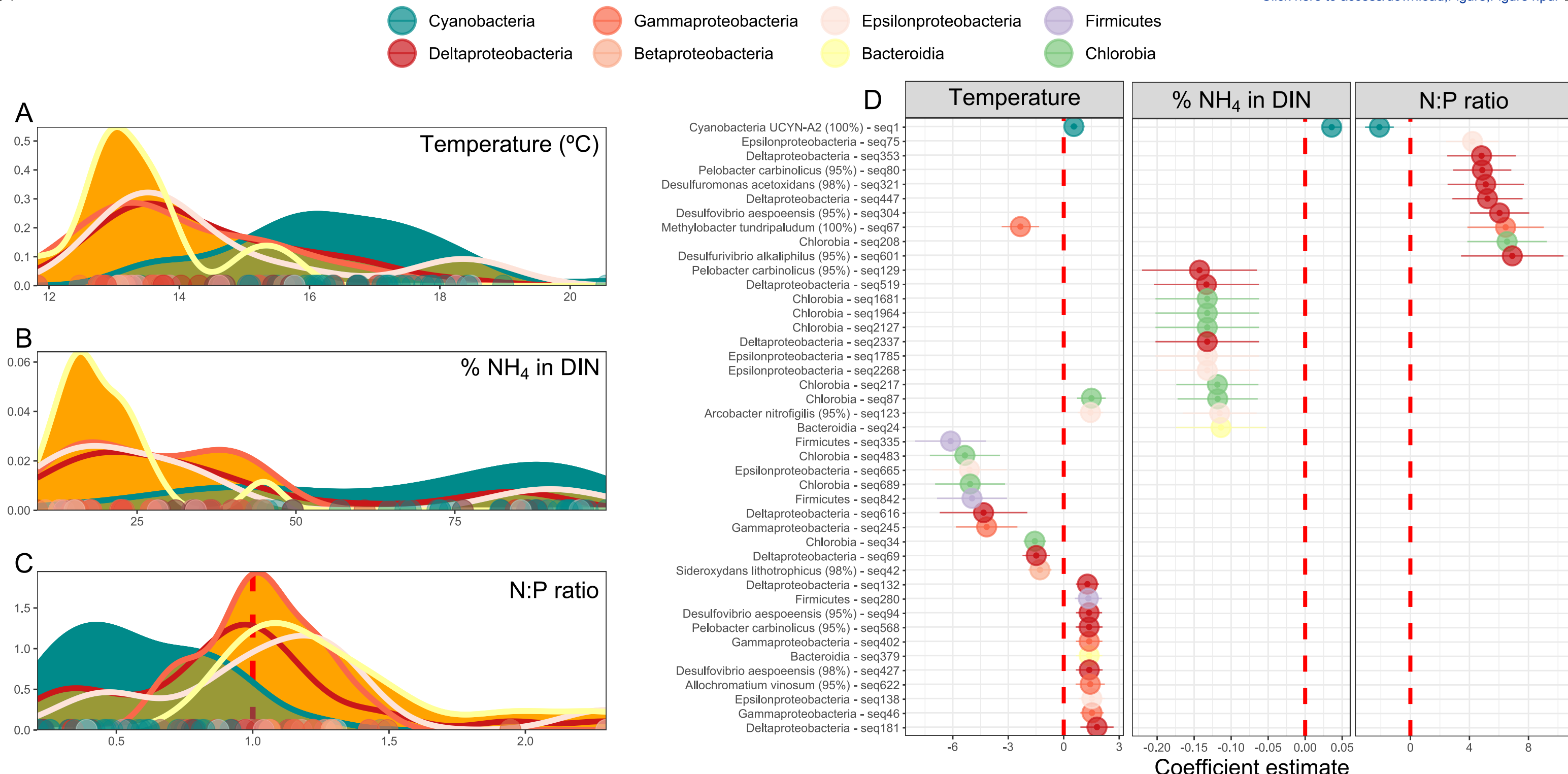
[Click here to access/download;Figure;Figure4.pdf](#)

Figure 5

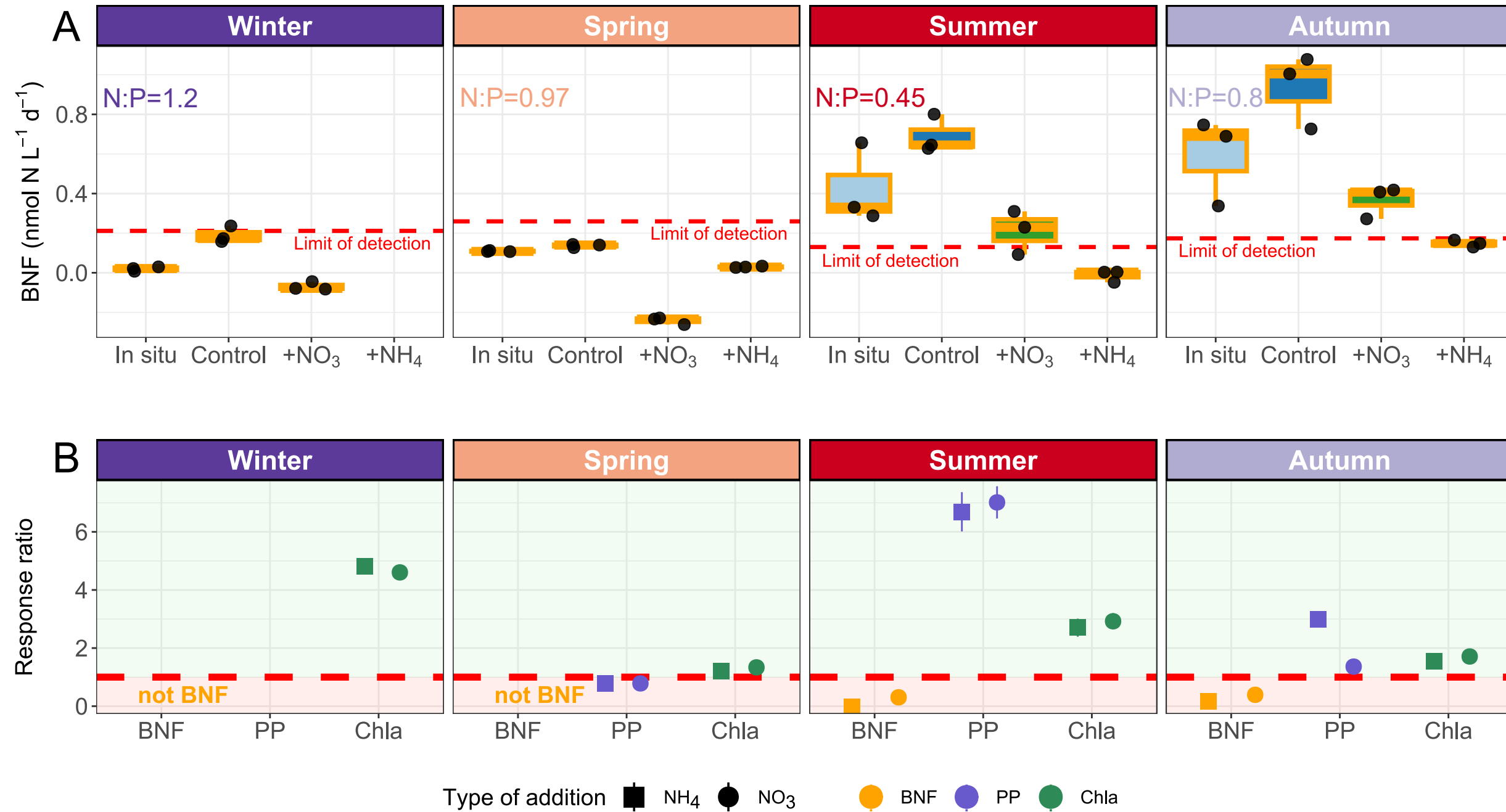
[Click here to access/download;Figure;Figure5.pdf](#)


Figure 6

Spring

Summer

Autumn

Winter

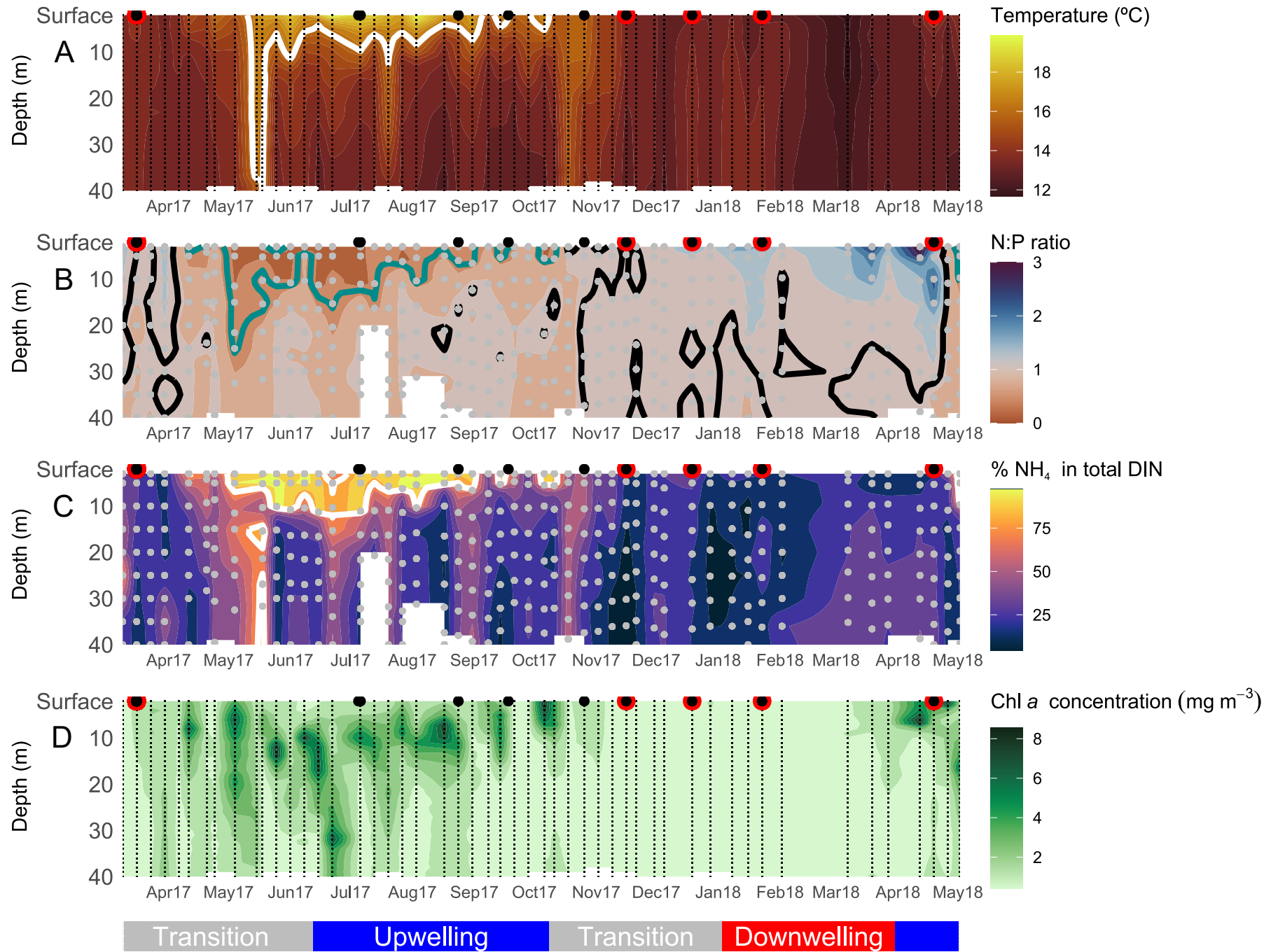
[Click here to access/download;Figure;Figure6.pdf](#)

Figure 7

Shelf, west of 9°W

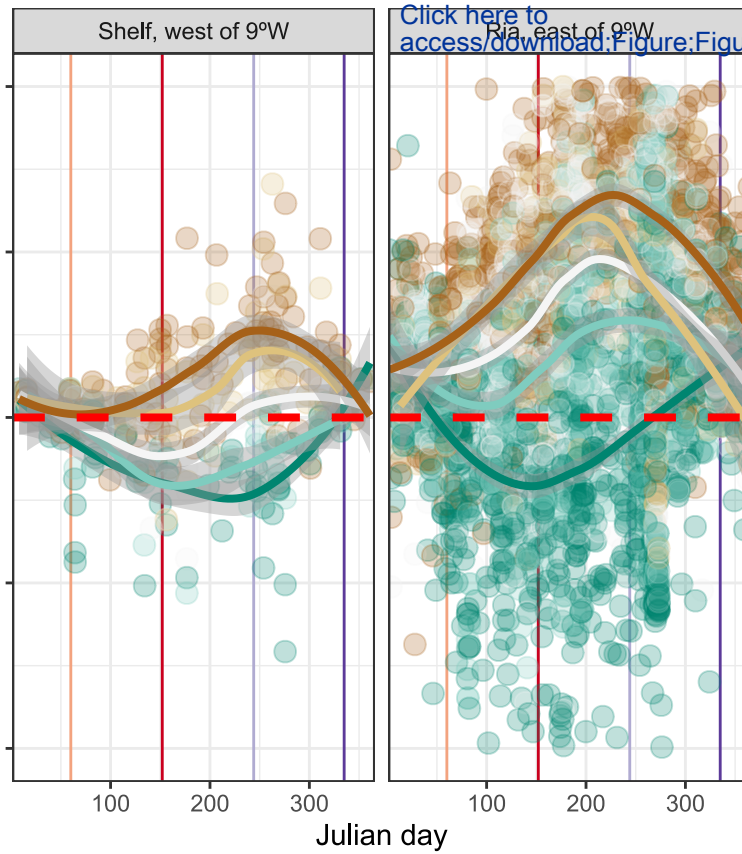
Click here to

Ria, east of 9°W

Apparent Oxygen Utilization (AOU, $\mu\text{mol kg}^{-1}$)100
50
0
-50
-100

100 200 300

Julian day



Depth

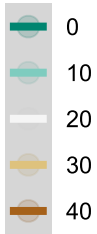
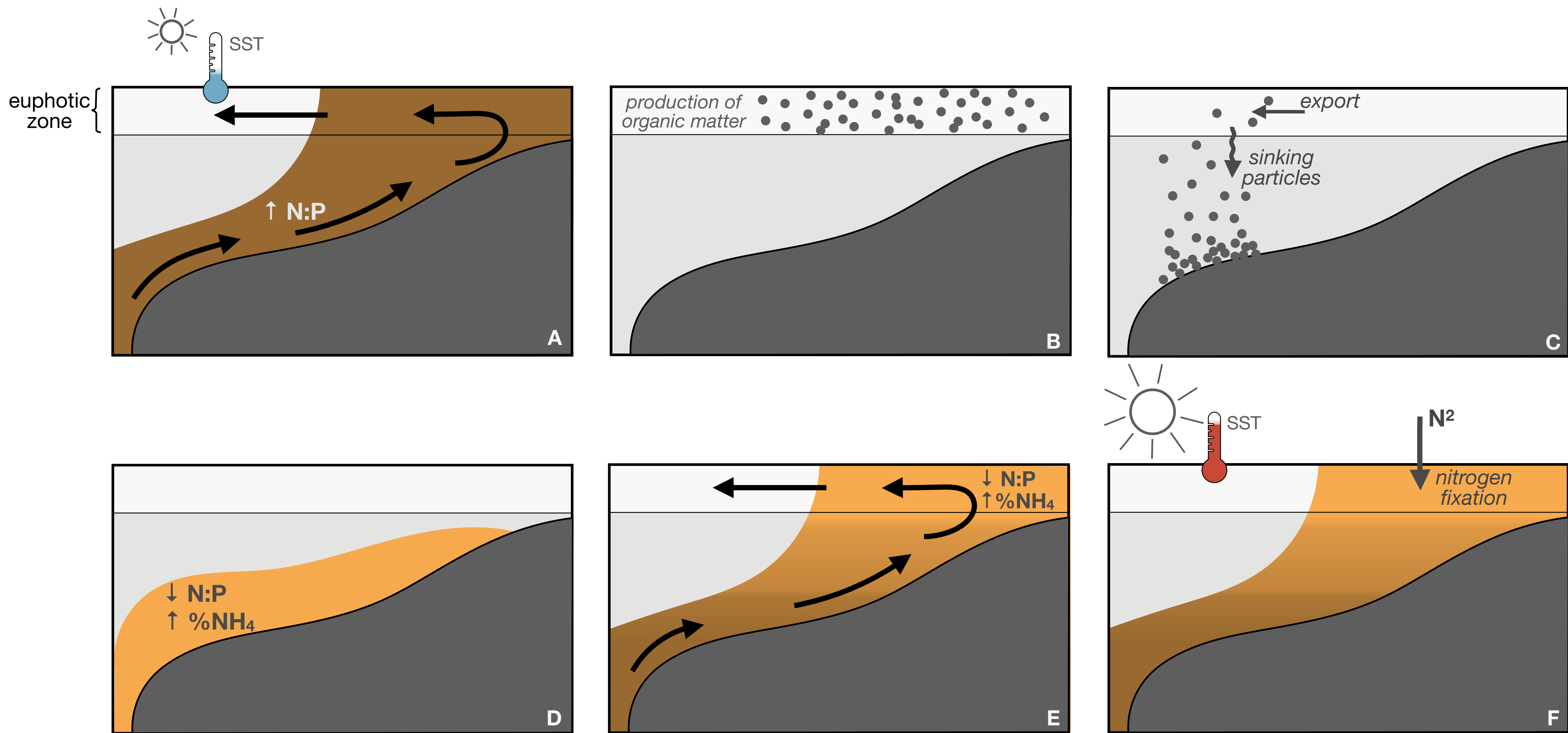


Figure 8

Click here to access/download;Figure;Figure8.pdf *





Click here to access/download
Supplemental Material
Fontela_SupplInfo.docx



Click here to access/download
Supplemental Material
Fontela_SuplInfoTableS5.xlsx